RAMAN AND FT-IR IMAGING OF *IN VIVO* DAMAGED TISSUE INDUCED BY 7, 12-DIMETHYLBENZANTHRACENE (DMBA) IN MOUSE MODELS[#]

ALEXANDRA FĂLĂMAŞ[*,***], *SIMONA CÎNTĂ-PÎNZARU*[*], *C. DEHELEAN*[**], *CH. KRAFFT*[***], *J. POPP*[***,****]

*Faculty of Physics, "Babeş-Bolyai" University, 1, Kogălniceanu st, 400084 Cluj-Napoca, Romania, alexandra.falamas@phys.ubbcluj.ro
** Faculty of Pharmaceutics, "Victor Babeş" University of Medicine and Pharmaceutics, 2, Eftimie Murgu Square, 300041 Timişoara, Romania
[***]Institute of Photonic Technology, Albert Einstein Straße 9, 07745 Jena, Germany
[****]Institute of Physical Chemistry, Helmholtzweg 4, 07743 Jena, Germany

Abstract. This paper presents a debut study of damaged tissues by 7, 12 dimethylbenzanthracene (DMBA) and UVB radiation. Before data acquisition samples were inoculated in formalin solution mixed with colloidal silver. The objective was to apply Raman, FT-IR and SERS spectroscopy to detect the structure and conformation of molecular components from tissues originating from wounded mouse models. These vibrational micro-spectroscopies can provide molecular information of the examined samples with a high spatial resolution at microscopic level. Raman imaging was applied to investigate areas from the tissues and identified SERS effect due to the added colloidal nanoparticles. The analysis of these spectra indicated chemisorption of the nanoparticles in the tissue.

Keywords: UV radiation, SERS, mouse model, silver nanoparticles.

INTRODUCTION

Raman spectroscopy is a powerful vibrational spectroscopic technique which has been applied in different biomedical applications [13, 15, 19, 23, 27]. Some of its advantages such as requirement of no or little sample preparation, high spatial resolution and molecular level information have made it attractive for *in vivo* and *in vitro* characterization of biological tissues. The principle is that Raman spectra probe molecular vibrations providing highly specific fingerprinting of the molecular structure and biochemical composition of cells and tissues. Since most

[#]This study was presented in the *National Conference of Biophysics*, Cluj-Napoca, October, 2009.

Received: October 2009;
in final form November 2009.

ROMANIAN J. BIOPHYS., Vol. 20, No. 1, P. 1–11, BUCHAREST, 2010

diseases are induced by biochemical processes including mutation and/or infection and are accompanied by molecular composition changes in the tissues, vibrational spectroscopic methods are reported to be useful tools for analyses being objective and rapid [15]. They provide the necessary information without external markers such as stains or radioactive labels.

FT-IR spectroscopy is a complementary technique to Raman spectroscopy, which has also proven to be a potent analytical tool for studying complex biological materials such as tissues, body fluids and cell cultures [3, 4, 6, 28, 30]. Mid IR spectroscopy is based on the absorption of radiation, typically in the 400 – 4000 cm^{-1} range which excites molecular vibrations. Biological macromolecules such as proteins, nucleic acids, and lipids have specific, fingerprint IR spectra in the wavenumber range 400–1800 cm^{-1}. Because these spectral fingerprints are directly determined by molecular structures and cellular chemistry, IR spectroscopy has been shown to have promising potential to detect abnormal changes in cells and tissues [5]. IR spectroscopic fingerprints can probe chemical compositions and compositional and structural changes in tissues and cells in real time without markers on the molecular level. Therefore, IR spectroscopy has been recognized as an analytical tool in medical diagnostics [5].

Raman spectroscopy suffers the disadvantage of extremely poor efficiency because of its low cross section. In the past two decades there has been a renewed interest in Raman techniques due to the discovery of surface-enhanced Raman scattering (SERS) effect, which results in strongly increased Raman signals when molecules are adsorbed on nanometer sized metallic structures. This concern in surface enhanced Raman techniques is due especially to the progress in nanoparticles fabrication, noble metal nanoparticles being recognized as SERS-active platforms that exhibit a Raman enhancement factor ranging from 10^6 to 10^{14} in appropriate surface plasmon resonance conditions. In order to increase the Raman intensity and to obtain a high specificity of the spectral response in analyzed samples, here we probed the SERS from skin tissue using silver colloidal nanoparticles and visible laser excitation [8, 24].

Based on SERS theory, if the Ag nanoparticles attached to the tissue, or if the laser spot falls at the junction between a nanoparticle and tissue, enhanced Raman signal should be observed. The strong enhancement of Raman scattering attributed to the SERS effect arises from combined electromagnetic and chemical mechanisms involving the adsorbate and the metal surface. The chemical effect is based on the adsorption of the molecules at certain surface sites, creating a charge-transfer state between the metal and the adsorbed scatterer. The electromagnetic effect appears because of the collective oscillations of the conduction electrons that result when a metal is irradiated with light. These electrons, also called “surface plasmons”, generate a secondary electromagnetic field, which can add to the incident one. This resonant response greatly enhances the local electromagnetic field intensity, thereby enhancing the efficiency of Raman scattering for molecules on or near the metal surface [1, 2, 7, 11, 19, 25].

The aim of this study was to apply vibrational spectroscopic techniques to study *in vivo* damaged tissue by UVB radiation and 7, 12 dimethylbenzanthracene (DMBA) solution in mouse models and to detect the structure and conformation of molecular components.

MATERIALS AND METHODS

SAMPLE PREPARATION

In this study two mice species (C57BL/6J and NMRI) and two rats of Sprague Dawley strain weighing 170–200 g were employed. The mice and one rat were exposed to UV radiation (295 nm) and all specimens were treated with DMBA solution, a synthetic polycyclic aromatic hydrocarbon which is known to induce cancer in different organs even it is applied topically. Autopsy tissue samples of about 0.5–1 cm^3 were collected from different tissues (lung, liver, skin). The samples were fixed in 10% formalin solution mixed with colloidal silver prepared through Lee-Meisel method.

Cryo-sections were cut from the formalin-fixed samples using a LEICA CM3050S cryostat and placed on CaF2 slides. The samples were not submitted to any preparation, like "freezing shock" in liquid nitrogen or washing.

All experimental procedures were approved by UMFT Bioethical Committee and institutional guidelines in the handling and care of the animals. The experiment is part of a larger study of three groups using eight animals for model and treatment with new formulations. The animals were accommodated to UMFT Biobase and they have been maintained in optimal conditions. The food was standard and was administered as the water, *ad libitum*. The day/night cycle was 12/12 hours and the humidity over 55%.

INSTRUMENTATION

Single spectra were collected from different regions from all samples placed on CaF2 slides. Spectra were recorded using a Raman microscope coupled to a 785 nm diode laser (Kaiser Optical Systems). The laser power was set to 200 mW. The exposure time was 5 seconds and each spectrum was an average of 2 accumulations. Raman maps were acquired using the same instrument, each map having a dimension of $19 \times 19 = 361$ spectra with a step size of 10 μm, exposure time 2 s per spectrum, number of acquisitions 2, dwell time between 10–30 s.

FT-IR images were acquired in transmission mode using an FT-IR microscope coupled to a 64×64 focal plane array detector (Varian). A typical FT-IR imaging acquisition consists of 4096 IR spectra taking 4 minutes. 40 scans at 4 cm^{-1} resolution were collected and Fourier transformed to produce the resulting spectrum from 950 to 4000 cm^{-1}. The dimensions of the images were 350×350 μm.

Data acquisition was controlled by the HoloMap module of the HoloGrams software package (Kaiser). The software automatically performs a cosmic ray correction and wavelength calibration.

DATA ANALYSIS

The resulting Raman and FT-IR images were processed using CytoSpec [31] software packages. An offset correction of each complete spectrum removed all negative intensities in the data set. Other preprocessing techniques included background subtraction, polynomial baseline correction and filtering. Low-intensity spectra were removed from the data sets because they corresponded to positions outside the tissue, near holes, near fissures or near margins. In both, FT-IR and Raman images, the intensity of the amide I band at 1656 cm^{-1} was used to determine whether some regions of the sample were too thin for the spectra to be included in the subsequent data analysis. Finally, clustering analysis was performed on the data sets.

Cluster analysis identifies regions of the sample that have similar spectral response by clustering the spectra into groups or clusters such that differences in the intra-cluster spectral responses are minimized while simultaneously maximizing the inter-cluster differences between spectral responses. The hierarchical cluster analysis (HCA) algorithm calculates the symmetric distance matrix (size n×n) between all considered spectra (number n) as a measure of their pairwise similarity. The algorithm then searches for the minimum distance, collects the two most similar spectra into a first cluster and recalculates spectral distances between all remaining spectra and the first cluster. In the next step the algorithm performs a new search for the most similar objects, which now can be spectra or clusters. The two most similar objects are clustered again and the distance values of the newly formed cluster are recalculated. This iterative procedure is repeated n–1 times until all spectra have been merged into one cluster.

RESULTS

Skin covers the surface of the body and has an important role in protecting it against different external factors. It consists essentially of three tissue layers: deep subcutaneous fatty layer, dermis and epidermis, the most superficial layer. Epidermis is a multi layer membrane which contains no blood vessels. Its outermost layer is stratum corneum which acts like a primary barrier to environmental contaminants.

Prolonged exposure to UV radiation can cause premature skin aging, skin cancer and a host of skin changes. Some of the possible mechanisms for UV skin damage are collagen breakdown and consistency changes, the formation of free radicals, interfering with DNA repair and inhibiting the immune system.

The mice and rats used in this study were exposed to UVB radiation (295 nm). After exposure, the skin manifested injury in a variety of ways, including both acute and chronic responses, the most evident feature of UV radiation being erythema (redness or sunburn). After one month of exposure, the visual aspects indicated important skin damages that suggested photoaging and first steps of skin carcinoma (Fig. 1).

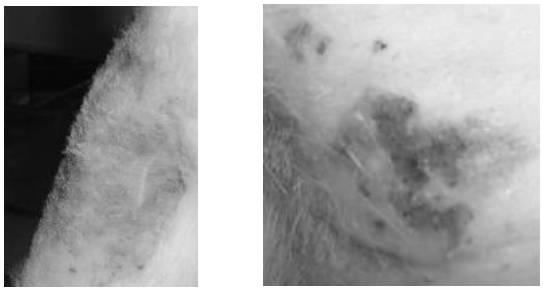

Fig. 1. Skin photodamage in evolution (left) after 4 weeks – erythema and (right) after 10 weeks – pre-carcinoma.

Skin samples, obtained from the specimens exposed to UVB radiation for 10 weeks, were submitted to histopathological investigations to get a precise insight on the nature of the damage. The results revealed different types of pathologies indicating skin damages and precancerous reactions. Some of the pathological initial conclusions pointed towards tissue destruction, hyperkeratosis with inflammatory infiltration, desmoplasic dermal reaction and increasing collagen fibers and blood tissues in dermis (Fig. 2).

For investigating the samples, the first step was to acquire single Raman spectra from all skin samples. Raman spectra can give important clues to understand the biochemical nature of specimens. The molecular fingerprint region, 700–1700 cm^{-1} is rich in spectral features characteristic to the main molecular components of tissues, proteins, lipids, nucleic acids and collagen, which is specific for skin samples (Fig. 3). Most of the contributions present in those spectra are proteins which can be seen at 622 (C–C twisting mode of phenylalanine), 644 (C–C twisting mode of tyrosine), 758 (symmetrical ring breathing of tryptophan), 852 (ring breathing of tyrosine), 920 (C–C stretching mode of proline), 938 (C–C stretch of protein backbone), 1002 (symmetrical ring breathing of phenylalanine), 1032 (CH in plane bending of phenylalanine), 1083 (C–N stretch of proteins, C–C and C–O stretch of phospholipids), 1155 (C–C and C–N stretching vibrations of proteins), 1173 (CH in plane bending of tyrosine), 1220–1280 amide III, 1320 (CH bending of proteins), 1446 (CH_2 bending of proteins), 1586 (phenylalanine) and 1657 cm^{-1} (amide I – C–O stretch of proteins, α-helix conformation, collagen and elastin). Other molecular components found here are lipids whose bands are present at 1063 (skeletal C–C stretch), 1083 (C–N stretch), 1127 (C–C stretch),

1266 (C–H in plane bending) and 1296 cm^{-1} (CH_2 bending vibrations). The increased content of collagen in skin gives bands at 852, 874, 940, 1244, 1319, and 1657 cm^{-1} [9, 12, 16, 20, 21, 22].

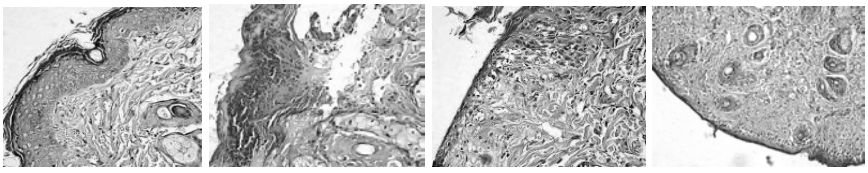

Fig. 2. Histological evaluations of skin lesions after 10 weeks of exposure. From left to right: normal skin; pathological-disposition of epithelial zone cubulous aspects and conjunctive tissue destruction in the second image, ulcerations, hyperkeratosis with an inflammatory infiltration, lesions in basal layer of epidermis, desmoplasic dermal reaction and increasing of collagen fibers in the third image and sub-epidermal densification, basal layer cells abundant, increasing of blood tissues in dermis, absence of keratinisation in the last one.

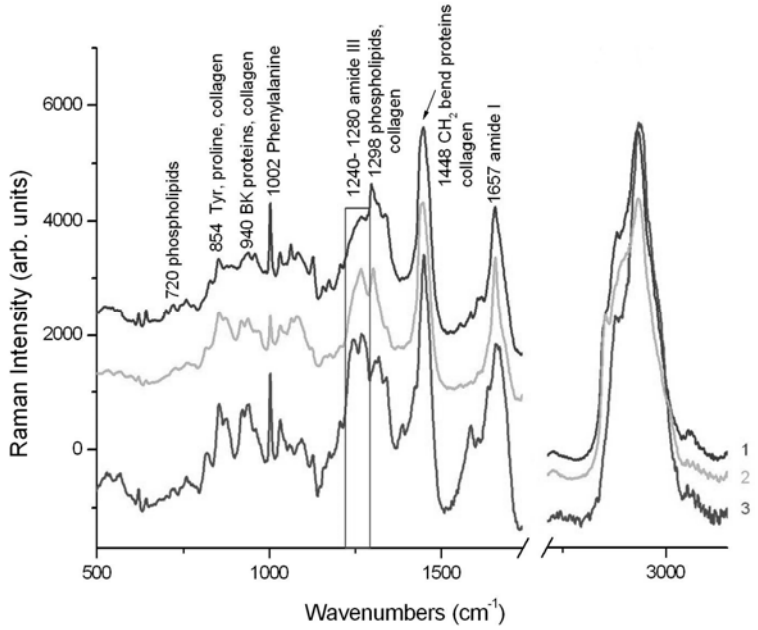

Fig. 3. Single Raman spectra of skin samples. (1) Raman spectrum of skin from C57BL/6J specimen, (2) skin from Sprague Dawley rat and (3) skin from NMRI mouse. The 500–1700 cm^{-1} wavenumber interval was magnified for better examination.

FT-IR spectroscopy has proven to be a powerful investigation tool for biomolecules to probe the structure of lipids, nucleic acids, carbohydrates and proteins [10, 29]. FT-IR imaging was applied for the investigation of the skin samples, collected from C57BL/6J and NMRI mouse specimens and from one

Sprague Dawley rat. The resulted data sets were subjected to HCA analysis using D-values method for calculating the distances between the objects and Ward's algorithm as the cluster method and the spectra were scaled at the amide I band in the 1620–1680 cm^{-1} interval. The imaging mode of IR spectrometers has a significant time advantage due to the multichannel focal plane array (FPA) detectors, which record thousands of spatial points of a globally illuminated area in a single measurement which takes only few minutes [17].

The results obtained for NMRI skin sample are shown here. The HCA analysis divided the selected area into three clusters. The representative spectra are presented in Fig. 4. All FT-IR spectra exhibit bands near 1068, 1231, 1385, 1455, 1540, 1656, 2851, 2920, 2955 and 3300 cm^{-1} characteristic of lipids, proteins, cholesterol and nucleic acids. The spectra are dominated by the amide I and II band at 1656 and 1537 cm^{-1} which arise from the C=O stretching and N–H bending of the amide group, the CH_2 asymmetrical stretching mode of lipids at 2924 cm^{-1} and the amide A band around 3296 cm^{-1}. The amino acid side chain from peptides and proteins at 1453 cm^{-1} was associated with the asymmetric and symmetric CH_3 bending vibrations. The 1234 cm^{-1} band indicates spectral contribution of compounds containing PO_2, CO, and CH_2 groups, typical for lipids. The bands located around 1453 and 1391 cm^{-1} are due to CH_2 and CH_3 bending of cholesterol and/or phospholipids.

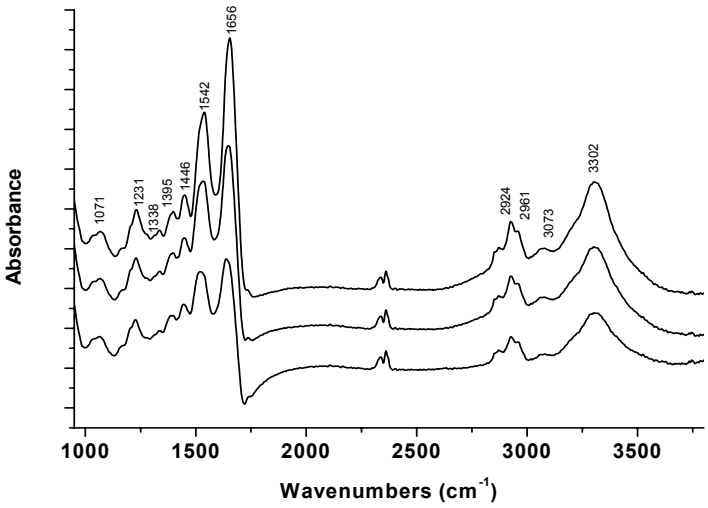

Fig. 4. IR spectra resulted after HCA analysis applied on an area from the skin sample of NMRI mouse specimen.

Besides investigating the molecular changes which occur in different organs upon exposure to UV irradiation and treatment with 7, 12-dimethylbenzanthracene (DMBA) solution, our aim was to inspect whether SERS effect can be detected in

those samples, considering the fact that the tissues were first immersed in formalin solution mixed with colloidal silver nanoparticles.

A specific area of 180 × 180 μm was chosen from the whole sample. This region was selected based on the density of the tissue. After the acquisition of the Raman image, cluster analyzing was performed on the resulted data set, using the HCA method implemented in CytoSpec program. Finally, the tissue was divided into three clusters. Three spectra representing each cluster are shown in Fig. 5.

The bottom spectrum is supposed to be a Raman spectrum because it coincides with the spectra in Fig. 3. However, the upper spectrum contains additional intense bands near 230, 500, 1211, 1316 and 1576 cm^{-1} which are consistent with the SERS effect.

To the best of our knowledge this is the first time when SERS effect, acquired from tissue samples prepared in this manner, is reported. Until now SERS effect was reported only for cells [14]. Previously, in literature, it was stated that SERS effect can also be acquired from PEG-lated gold nanoparticles injected into subcutaneous and deep muscular sites in live animals. The signal was acquired *in vivo* from the point where the nanoparticles were injected. Also, SERS detection was reported for *in vivo* cancer targeting, using antibody conjugated gold nanoparticles that recognize the tumor biomarker [25].

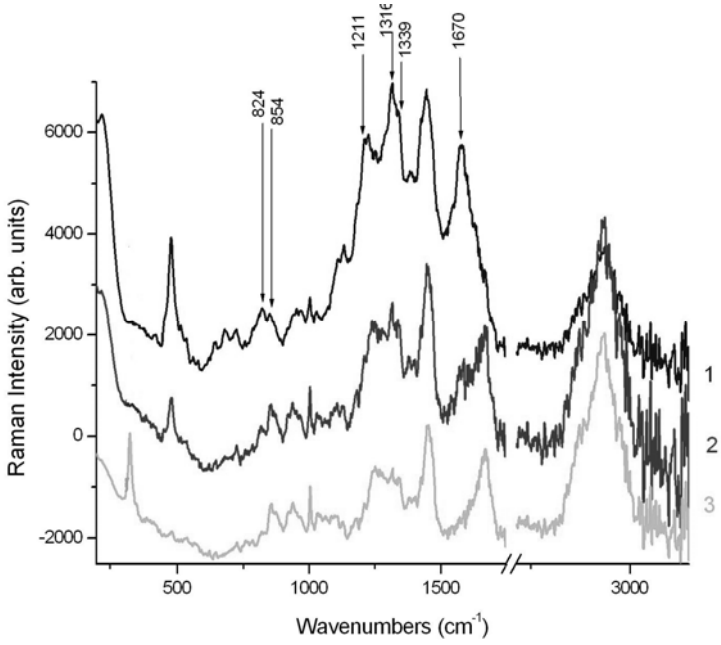

Fig. 5. Representative averaged-clustered spectra resulted after HCA analysis, applied on the same area of the NMRI skin sample used for FT-IR investigations.

One problem lies in the reproducibility of the recorded SERS spectra. SERS variability was evident in many ways. The intensity varied from one point of acquisition to another during the Raman image and also, the resulted signals showed differences in peak locations (Fig. 6). The spectral signatures are different from the Raman spectra in Fig. 3 and the SERS spectra in Fig. 5. One possible explanation is that certain frequencies of scattering are more sensitive to the enhancement than others. Additionally, different portions of the tissue could have been subjected to the enhancement during the measurement. Depending on how many adsorbed molecules on the Ag nanoparticles does the spot of the laser encompass, the spectra can present a lot of fluctuations in signal intensities and frequencies. This could be an explanation for the fact that in the resulted SERS spectra after Raman imaging, there are differences in the way the present modes are amplified.

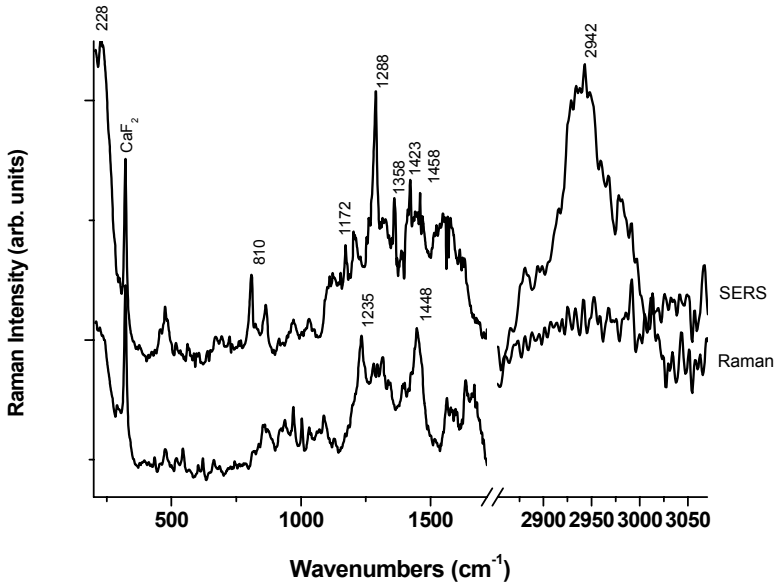

Fig. 6. SERS spectrum recorded during Raman imaging in comparison with a Raman spectrum acquired from the point next to it.

CONCLUSIONS

In this study we have demonstrated the capacity of Raman and FT-IR spectroscopy of detecting the nature of molecular components of the *in vivo* damaged tissues by UVB radiation and DMBA solution from mouse and rat specimens. Raman and FT-IR imaging were applied to investigate specific areas from the autopsy tissues collected from different mice specimens. In this way, the

SERS effect was identified. This was expected due to the colloidal nanoparticles which were mixed with the formalin solution in which the samples were immersed.

By inoculating Ag colloidal nanoparticles in biological tissues, we have proved here the possibility of recording SERS spectra which can be used to investigate the nature of the molecular components of biological samples.

SERS effect could be the answer to the search and need for new technologies for obtaining biochemical information from biological samples, which give excellent sensitivity, maximum chemical information content and quantitatively reproducible signals. The SERS fingerprint of a tissue is sensitive to subtle chemical changes inside it and can be used to study those chemical modifications that take place. SERS can be a valuable and powerful approach to the identification of chemical components in tissues through reproducible acquisitions under controlled experimental conditions.

Acknowledgment. We acknowledge financial support from the PN II– IDEI grants of CNCSIS, Romania. One of the authors, A.F., highly acknowledges Prof. Jürgen Popp and Prof. Christoph Krafft from IPHT, Jena, for their support.

REFERENCES

1. ALBRECHT, M.G., J.A. CREIGHTON, Anomalously intense Raman spectra of pyridine at a silver electrode, *J. Electroanal. Chem.*, 1977, **99**(15), 5215–5217.
2. AROCA, R., *Surface Enhanced Vibrational Spectroscopy*, Wiley&Sons, West Sussex, UK, 2006**.**
3. DELERIS, G., C. PETIBOIS, Applications of FT-IR spectrometry to plasma contents analysis and monitoring, *Vib. Spectrosc.*, 2003, **32**, 129–136.
4. DIEM, M., S.S.M. BOYDSTON-WHITE, L. CHIRIBOGA, Infrared spectroscopy of cells and tissues: Shining light onto a novel subject, *Applied Spectroscopy*, 1999, **53**, 148–161.
5. DUKOR, R.K., Vibrational Spectroscopy of the Detection of Cancer. Handbook of Vibrational Spectroscopy, in: *Applications of Vibrational Spectroscopy in live and natural Sciences*, Five volume set, John Wiley&Sons LTD, 2002, pp. 3335–3361.
6. ERUKHIMOVICI, V., M. TALYSHINSKY, Y. SOUPRUN, M. HULEIHEL, Spectroscopic characterization of human and mouse primary cells, cell lines and malignant cells, *Photochem. Photobiol*., 2002 **76**, 446–451.
7. FLEISCHMANN, M., P.J. HENDRA, A.J. MCQUILLAN, Raman spectra of pyridine adsorbed at a silver electrode, *Chem. Phys. Lett*., 1974, **26**, 163–166.
8. HERING, K., CIALLA, D., ACKERMANN, K., DOERFER, T., R. MOELLEER, H. SCHEIDEWIND, R. MATTHEIS, W.R. FRITZSCHE, P. ROESCH, J. POPP, SERS: a versatile tool in chemical and biochemical diagnostics, *Analytical and Bioanalytical Chemistry*, 2008, **390**(1), 113–124.
9. HUNAG, Z., A. MCWILLIAMS, H. LUI, D.I. MCLEAN, S. LAM, H. ZENG, Near-infrared Raman spectroscopy for optical diagnosis of lung cancer, *Int. J. Cancer*, 2003, **107**, 1047–1052.
10. JACKSON, M., H.H. MANTSCH, Protein secondary structure from FT-IR spectroscopy: Correlation with dihedral angles from three-dimensional Ramachandran plots, *Can. J. Chem*., 1991, **69**, 1639–1642.
11. JEANMAIRE, D.L., R.P. VAN DUYNE, Surface Raman electrochemistry. Part I. Heterocyclic, aromatic and aliphatic amines adsorbed on the anodized silver electrode, *J. Electroanal. Chem.*, 1977, **84**, 1–20.

12. KAST, R.E., G.K. SERHATKULU, A. CAO, A.K. PANDYA, H. DAI, J.S. THAKUR, V.M. NAIK, R. NAIK, M.D. KLEIN, G.W. AUNNER, R. RABAH, Raman spectroscopy can differentiate malignant tumors from normal breast tissue and detect early neoplastic changes in a mouse model, *Biopolymers*, 2008**, 89**(3), 235–241.
13. KENDALL, C., M. ISABELLE, F. BAZANT-HEGEMARK, J. HUTCHINGS, L. ORR, J. BABRAH, R. BAKER, N. STONE, Vibrational spectroscopy: a clinical tool for cancer diagnostics, *Analyst*, 2009, **134**, 1029–1045.
14. KNEIPP, J., H. KNEIPP, A. RAJADURAI, R.W. REDMOND, K. KNEIPP, SERS label for optical probing and imaging of single live cells*., J. Raman Spectrosc*., 2009, **40**, 1–5.
15. KRAFFT, C.H., B. DIETZEK, J. POPP, Raman and CARS microspectroscopy of cells and tissues, *Analyst*, 2009, **134**, 1046–1057.
16. KRAFFT, C., D. CODRICH, G. PELIZZO, V. SERGO, Raman and FTIR microscopic imaging of colon tissue: a comparative study., *J of Biophotonics*, 2008, **1**(2), 154–169.
17. KRAFFT, C.H., M. KIRSCH, C. BELEITES, G. SCHACKERT, R. SALZER, Methodology for fiber-optic Raman mapping and FTIR imaging of metastases in mouse brains, *Anal. Bioanal. Chem*., 2007, **389**, 1133–1142.
18. MIN, Y.K., T. YAMAMOTO, E. KOHDA, T.M. ITO, H-O. HAMAGUCHI, 1064 nm near-infrared multichannel Raman spectroscopy of fresh human lung tissues, *J. Raman Spectrosc.*, 2005; **36**, 73–76.
19. MOSKOVITS, M., Surface-enhanced spectroscopy, *Reviews of Modern Physics*, 1985, **57**(3), 783–824.
20. MUNTEAN, C.M., A. HALMAGYI, M.D. PUIA, I. PAVEL, FT-Raman of genomic DNA from plant tissues, *Spectroscopy*, 2009, **23**, 59–70.
21. NOTINGHER, I., Raman spectroscopy cell-based biosensors, *Sensors*, 2007, 7, 1343–1358
22. NOTINGHER, I., S. VERRIER, S. HAQUE, J.M. POLAK, L.L. HENCH, Spectroscopic study of human hung epithelial cells (A549) in culture: Living cells versus dead cells, *Biopolymers* (*Biospectroscopy*), 2003, **72**, 230–240.
23. PETRY, R., M. SCHMITT, J. POPP, Raman Spectroscopy – A prospective tool in the life sciences, *Chem. Phys. Chem.*, 2003, **4**, 14–30.
24. PINZARU-CINTA, S., L.M. ANDRONIE, I. DOMSA, O. COZAR, S. ASTILEAN, Bridging biomolecules with nanoparticles: surface-enhanced Raman scattering from colon carcinoma and normal tissue, *J. Raman Spectrosc.*, 2008, **39**, 331–334.
25. QIAN, X., X-H. PENG, D.O. ANSARI, Q. YIN-GOEN, G.Z. CHEN, D.M. SHIN, L. YANG, A.N. YOUNG, D. MAY, M.D. WANG, S. NIE, *In vivo* tumor targeting and spectroscopic detection with surface-enhanced Raman nanoparticle tags, *Nature Biotechnology*, 2008, **26**, 83–90
26. QIAN, X.M., S.M. NIE, Single-molecule and single-nanoparticle SERS: from fundamental mechanisms to biomedical applications, *Chem. Soc. Rev*., 2008, **37**, 912–920.
27. SCHMITT, M., J. POPP, Raman spectroscopy at the beginning of the 21st century, *J. Raman Spectrosc.*, 2006, **37**, 20–28.
28. WANG, Y., R.I. BOYSEN, B.R. WOOD, M. KANSIZ, D. MCNAUGHTON, M.T.W. HEARN, *Biopolymers*, 2008, **89**, 895–905.
29. WANG, X.Y., J.M. GARIBALDI, B. BIRD, M.W. GEORGE, *Applied Intelligence*, 2007, **27**, 237–248.
30. WONG, P.T.T., High-pressure FT-IR spectroscopy for biomedical and cancer research, *Proc. AIP*, 1993, **309**, 1431–1434.
31. ***CytoSpec – an application for FT-IR spectroscopy imaging, www.cytospec.com.